NANOSTRUCTURES

An aqueous preoxidation method for monolithic perovskite electrocatalysts with enhanced water oxidation performance

Bo-Quan Li,* Cheng Tang,* Hao-Fan Wang, Xiao-Lin Zhu, Qiang Zhang†

Perovskite oxides with poor conductivity call for three-dimensional (3D) conductive scaffolds to demonstrate their superb reactivities for oxygen evolution reaction (OER). However, perovskite formation usually requires high-temperature annealing at 600° to 900°C in air, under which most of the used conductive frameworks (for example, carbon and metal current collectors) are reductive and cannot survive. We propose a preoxidization coupled electrodeposition strategy in which Co^{2+} is preoxidized to Co^{3+} through cobalt Fenton reaction in aqueous solution, whereas the reductive nickel framework is well maintained during the sequential annealing under nonoxidative atmosphere. The in situ–generated Co^{3+} is inherited into oxidized perovskites deposited on 3D nickel foam, rendering the monolithic perovskite electrocatalysts with extraordinary OER performance with an ultralow overpotential of 350 mV required for 10 mA cm^{-2}, a very small Tafel slope of 59 mV dec^{-1}, and superb stability in 0.10 M KOH. Therefore, we inaugurate a unique strategy for in situ hybridization of oxidative active phase with reductive framework, affording superb reactivity of perovskite electrocatalyst for efficient water oxidation.

INTRODUCTION

Growing consumption of energy and exhausting fossil fuels starve for sustainable energy systems (*1*–*3*). Fuel cells, metal-air batteries, and water splitting techniques are promising candidates for future energy supplements. However, their energy efficiencies are strongly limited by oxygen evolution reaction (OER) (*4*–*9*). The four-electron OER process ($4OH^- \rightarrow O_2 + 2H_2O + 4e^-$) is kinetically sluggish (*10*), strongly requiring electrocatalysts for accelerating water oxidation and lowering the overpotential. Precious metal oxides, such as IrO_2 and RuO_2, are well established as the state-of-art OER catalysts with super reactivity (*11*, *12*), but scarcity, high cost, and poor durability strongly limit their practical applications. Recently, various transition metal compounds have been investigated as a focus of highly effective and cost-efficient OER catalysts (*13*–*18*). In particular, perovskite oxides with tunable constitutions and structures have been widely recognized as a promising substitute (*19*–*26*).

To establish the catalytic system with high OER performance, intrinsic OER reactivity, well-regulated nanostructure, high conductivity, and strong coupled interface with low resistance are focused as main issues. Perovskite oxides exhibit superb OER reactivity comparable to that of precious metal oxides (*22*), but they have a morphology that is hard to control and conductivity that is very poor. The addition of conductive agents, such as Ketjenblack carbon (*27*), carbon black (*28*), graphene (*29*–*31*), carbon nanotubes (*32*, *33*), etc., by simple mechanical mixing usually leads to an improved conductivity and enhanced performance. Nevertheless, it still remains a great challenge to efficiently regulate the nanoscale morphology of perovskite oxides and integrate the active sites with conductive scaffolds at the same time, thereby limiting the full demonstration of their intrinsic OER activity. Controlled synthesis of nanosized perovskite oxide particles with abundant active sites and, simultaneously, in situ hybridization into hierarchical porous conductive frameworks with strong interaction are expected to optimize the perovskite oxide–based catalysts (*34*, *35*). However, perovskite oxides are dominantly achieved through high-temperature annealing at 600° to 900°C under an oxidative atmosphere. In this case, most reductive frameworks (for example, carbon and metal current collector) will be oxidized and destroyed with the loss of conductivity and continuous frameworks. Consequently, there is an intrinsic contradiction in the in situ hybridization of oxidative perovskite oxides with reductive conductive frameworks. Notably, this intrinsic contradiction is particularly common for OER catalytic systems because most OER electrocatalysts are oxidative and hard to be hybridized in situ.

In general, most of the conductive agents can be well preserved in an aqueous solution even with weak oxidative agents. On the basis of this consideration, the creation of oxidative perovskite precursors onto reductive scaffolds through preoxidation and inert annealing is proposed. To verify this concept, a typical perovskite oxide for OER, $LaCo_{0.8}Fe_{0.2}O_3$ (LCFO), is selected as the model perovskite (*29*), three-dimensional (3D) nickel foam (NF) is used as the conductive scaffold (*15*, *36*), and electrodeposition serves as a facile but effective in situ synthetic method to achieve a monolithic electrode with tunable active phases (*37*–*39*). Specifically, LCFO perovskites require trivalent Co species, but the Co precursor is always divalent under normal conditions. To achieve the required oxidative state of Co and protect the conductive scaffolds, Co^{2+} is preoxidized to Co^{3+} in an aqueous solution, whereas the reductive Ni scaffold is well maintained. As illustrated in Fig. 1, the as-obtained Co^{3+} then undergoes localized precipitation along with La^{3+} and Fe^{3+} through electrodeposition. Sequentially, the as-prepared hybrids consisting of oxidized perovskite hydroxide precursors and conductive frameworks are chemically stable under Ar protection during calcination at 700°C, resulting in a hybrid electrocatalyst with oxidized perovskite oxides onto the monolithic reductive nickel current collector. We demonstrated that the hybrid electrocatalyst exhibited superb OER reactivity with a low overpotential and outstanding durability in alkaline solution.

RESULTS

We fabricated the hybrid of NF/$LaCo_{0.8}Fe_{0.2}O_3$ through the preoxidation strategy (see more details in Materials and Methods). A red-colored

Beijing Key Laboratory of Green Chemical Reaction Engineering and Technology, Department of Chemical Engineering, Tsinghua University, Beijing 100084, China.
*These authors contributed equally to this work.
†Corresponding author. Email: zhang-qiang@mails.tsinghua.edu.cn

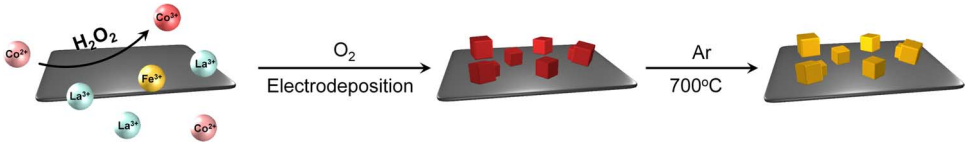

Fig. 1. In situ fabrication of the NF/oLCFO-Ar hybrid through electrodeposition coupled with oxygen reduction reaction and cobalt Fenton process, followed by calcination under Ar protection.

NF/perovskite hydroxide intermediate was fabricated first (Fig. 2A), and the monolithic precursor was then annealed at 700°C in Ar to obtain crystallized perovskite oxide (named as NF/oLCFO-Ar, where "o" marks the preoxidation in aqueous solution). The nanosized perovskite oxide particles are uniformly distributed onto the NF surface (Fig. 2B). Both scanning electron microscopy (SEM) (Fig. 2C) and transmission electron microscopy (TEM) images (Fig. 2D) demonstrate the oLCFO as homogeneous cubic nanoparticles with a size range of 20 to 50 nm, which is much smaller than those achieved by routine synthesis methods, such as sol-gel (*31*, *40*), solid-state reaction (*41*), and combustion (*42*). These nanosized perovskite oxides have more exposed atoms at the surface for water oxidation. The detailed perovskite structure was further confirmed by a high-resolution TEM image (Fig. 2E) and x-ray diffraction (XRD) pattern (Fig. 2F).

To further identify the state of La, Co, and Fe in oLCFO, both x-ray photoelectron spectroscopy (XPS) (fig. S1) and energy dispersive spectroscopy (EDS) analysis (fig. S2) were performed. All the required elements are unambiguously confirmed with expected atomic ratios of Co to Fe determined to be 3.7 and 4.2 by XPS and EDS, respectively. EDS mapping (fig. S3) further demonstrates a uniform distribution of La, Co, and Fe in the perovskite oxide. Considering the nanosized morphology, well-crystallized structure, and uniform distribution of the perovskite oxide together, the as-obtained monolithic NF/oLCFO-Ar is expected to have remarkable characters for superb OER reactivity.

The OER performance was probed using a three-electrode system in O_2-saturated 0.10 M KOH aqueous solution at room temperature. Figure 3A presents the *iR*-compensated linear sweep voltammetry (LSV) curves. Compared with bare NF, the OER current density of NF/oLCFO-Ar distinctly increases, indicating a significantly improved OER activity. The OER overpotential required to achieve a current density of 10 mA cm^{-2} (η_{10}) is 350 mV, which is among or even better than the reported OER electrocatalysts (table S1) (*22*, *26*, *33*, *34*, *43*–*46*). Notably, bare NF exhibits an obvious redox peak around 1.41 V versus reversible hydrogen electrode (RHE) in the polarization profile, which is assigned to the oxidation current of Ni. In contrast, the redox peak of Ni of NF/oLCFO-Ar can hardly be detected, implying the full covering of perovskite oxides as a porous active phase on the NF surface (Fig. 2B), thereby reducing the exposure and oxidation of NF in the electrolyte and fully using the conductivity of NF. In addition, NF/oLCFO-Ar has a much lower Tafel slope (59 mV dec^{-1}) than that of NF (144 mV dec^{-1}), demonstrating a more rapid kinetics for OER (Fig. 3B). The stability test was carried out at a constant potential required for an initial current of 2.0 mA cm^{-2}. The current density of NF/oLCFO-Ar scarcely decayed for 10,000 s (Fig. 3C), indicating superb durability. Consequently, NF/oLCFO-Ar demonstrates promising OER activity and stability, suggesting its potential for practical applications in water splitting and metal-air batteries.

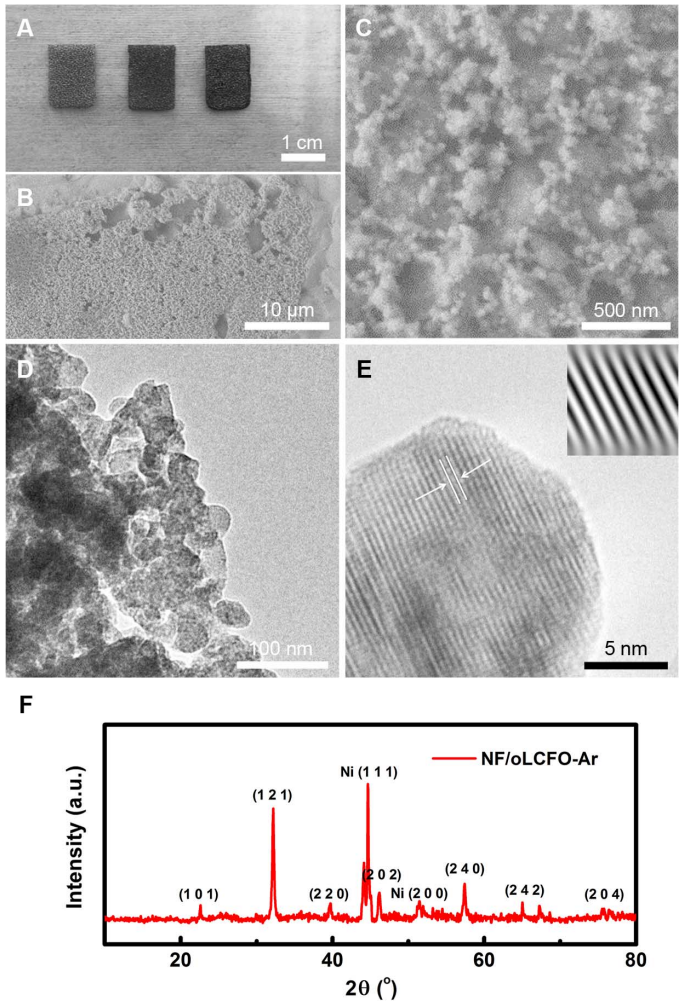

Fig. 2. Characterization of monolithic NF/oLCFO-Ar electrocatalysts. (**A**) Micrograph of bare NF, NF/oLCFO precursor after electrodeposition, and final NF/oLCFO-Ar electrocatalyst. (**B** and **C**) SEM and (**D** and **E**) TEM images and (**F**) XRD pattern of NF/oLCFO-Ar. a.u., arbitrary units.

DISCUSSION

It is expected that the promising OER activity and stability of NF/oLCFO-Ar are highly dependent on the effective fabrication strategy and the strongly coupled nanostructures. If the perovskite oxide oLCFO is physically postcoated onto a NF with the same loading amount of the active phase, the NF + oLCFO electrocatalyst exhibits a much lower current density compared with NF/oLCFO-Ar hybrids (Fig. 4A). Notably, the redox peak of Ni oxidation is clearly observed in this case, indicating a direct exposure of NF due to the chaotic distribution of perovskite particles, which is also confirmed by the SEM image shown in fig. S4 (A to C) with similar morphology (fig. S4, D and E) and stoichiometry (fig. S5) of perovskite nanoparticles. In addition, the Tafel slope (139 mV dec^{-1}) (fig. S6A) and stability (fig. S6B) of NF + oLCFO are greatly inferior to those of

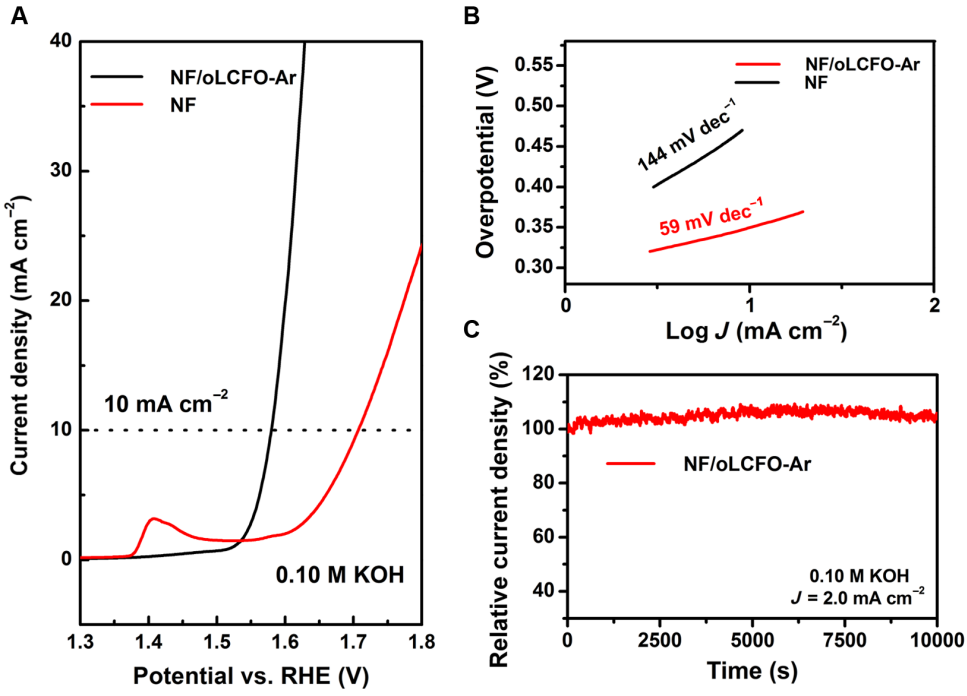

Fig. 3. OER performance of NF/oLCFO-Ar and the control sample NF in O_2-saturated 0.10 M KOH. (**A**) *iR*-compensated LSV profiles at a scan rate of 10.0 mV s^{-1}. (**B**) Tafel slope and (**C**) chronoamperometric response at a constant potential required for an initial current density of 2.0 mA cm^{-2}.

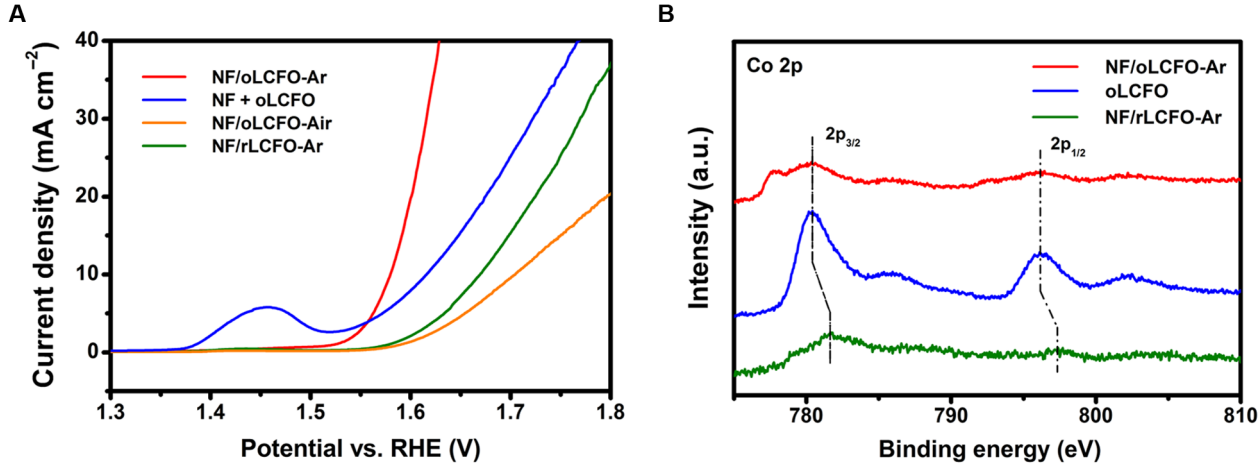

Fig. 4. Evaluation of in situ hybrid structure and preoxidation strategy. (**A**) LSV profiles of NF/oLCFO-Ar, NF + oLCFO, NF/oLCFO-Air, and NF/rLCFO-Ar. (**B**) Co 2p XPS spectra of NF/oLCFO-Ar, oLCFO perovskite nanoparticles for NF + oLCFO and NF/oLCFO-Air, and NF/rLCFO-Ar.

NF/oLCFO-Ar, suggesting the necessity of in situ hybridization realized by electrodeposition.

In general, cobalt in perovskite oxides with higher oxidation states is favorable for better OER reactivity (*47*–*49*). The routine strategy is to calcine the perovskite precursors in oxidative atmospheres (such as air) to transform Co^{2+} to Co^{3+}. However, as it is mentioned, there is an intrinsic contradiction of the oxidative perovskite oxides and the reductive NF framework under high temperature in air. If the NF/perovskite hydroxide precursor was directly annealed in air, NF was apparently oxidized to nickel oxide with a collapsed framework and notorious cracks (fig. S7). The OER catalysis of NF/oLCFO-Air shows poor performances with a high overpotential of 470 mV for 10 mA cm^{-2}, a large Tafel slope of 78 mV dec^{-1}, and a very brittle stability (Fig. 4A and fig. S6).

To further understand the facile synthetic method for in situ hybridization of NF/oLCFO, a supposed mechanism is proposed. As detailed in Scheme 1, H_2O_2 is first generated through a two-electron oxygen reduction reaction (ORR) in the O_2-saturated aqueous electrolyte. The H_2O_2 affords oxidative intermediates at a reductive potential on NF scaffold (Scheme 1A), and Co^{2+} is then oxidized to Co^{3+} by H_2O_2 through Fenton reaction (Scheme 1B). Meanwhile, NO_3^- is reduced to NH_4^+ at the surface of NF, providing a local alkaline environment by generating OH^- (Scheme 1C) (*50*, *51*). The as-oxidized Co^{3+}, along

$$O_2 + 2H_2O + 2e^- \rightarrow H_2O_2 + 2OH^- \quad (A)$$

$$H_2O_2 + 2Co^{2+} \rightarrow 2Co^{3+} + 2OH^- \quad (B)$$

$$NO_3^- + 7H_2O + 8e^- \rightarrow NH_4^+ + 10OH^- \quad (C)$$

$$xLa^{3+} + yCo^{3+} + zFe^{3+} + wOH^- \rightarrow oLCF(OH) \quad (D)$$

Scheme 1. Proposed mechanism of preoxidation synthesis of NF/perovskite hydroxide precursor.

with La^{3+} and Fe^{3+}, then coprecipitates with the locally generated OH^- to form a perovskite hydroxide precursor (Scheme 1D). Then, the moderate annealing in Ar transforms the hydroxides into crystallized perovskite oxides, which are strongly coupled onto the reserved NF substrate. Coupling the ORR process, cobalt Fenton reaction, and electrodeposition reaction sequentially, the preoxidized perovskite oxide precursor is in situ–synthesized with cobalt in trivalent state.

To further confirm the role of H_2O_2 intermediate as oxidant for Co^{3+} formation and verify the proposed mechanism, another control sample electrodeposited in N_2-saturated electrolyte with other conditions unaltered was fabricated and named as NF/rLCFO-Ar (fig. S8). As indicated by the XPS spectrum of NF/rLCFO-Ar, the Co oxidation state in this sample is +2 (Fig. 4B). In contrast, perovskite oxides of NF/oLCFO-Ar synthesized through preoxidation in O_2-saturated electrolyte and oLCFO perovskite oxide nanoparticles for NF + oLCFO and NF/oLCFO-Air obtained by direct annealing in air afford +3 oxidation state of Co, identified by the shift to lower binding energy in the XPS spectra (*52*). As expected, the OER performance of NF/rLCFO-Ar is much poorer compared with NF/oLCFO-Ar in all criteria (Fig. 4A and fig. S6A). This observation unambiguously confirms the fact that the in situ–generated H_2O_2 in O_2-saturated solution provides Co^{3+}-containing compounds for highly active perovskite formation. Considering the similar perovskite oxide phase (figs. S8 and S9) and composition (figs. S10 and S11) of NF/rLCFO-Ar and NF/oLCFO-Ar, the cobalt oxidation state is speculated as the most important ingredient for superb water oxidation reactivity. Consequently, preoxidation of metal precursors is crucial for the novel electrodeposition of active perovskite oxides, making it possible to rationally hybridize monolithic reductive NF and oxidative oLCFO toward superb OER performance.

In summary, we fabricated a monolithic NF/perovskite oxide hybrid via a novel electrodeposition method for enhanced OER performance. The proof-of-concept aqueous preoxidation strategy is proposed to overcome the intrinsic contradiction between oxidative perovskite oxides and reductive conductive frameworks in the in situ hybridization process. The in situ–generated H_2O_2 through ORR oxidizes Co^{2+} to Co^{3+} through cobalt Fenton process, providing the possibility for the generation and stabilization of Co^{3+} into solid perovskite phase. The as-synthesized NF/oLCFO-Ar has a uniform distribution of 20 to 50 nm perovskite oxides on the NF surface and exhibits superb OER performances with an ultralow overpotential (350 mV at 10 mA cm^{-2}), a very small Tafel slope (59 mV dec^{-1}), and extraordinary stability in 0.10 M KOH electrolyte. This work not only provides a new and promising material platform for super active OER electrocatalysts but also inaugurates an effective method to rationally integrate oxidative active phase with reductive framework.

MATERIALS AND METHODS

Synthesis of the electrocatalysts

The NF/oLCFO-Ar was synthesized through an in situ electrodeposition method under an O_2-saturated condition followed by thermal treatment. Typically, a NF (1.5 cm × 1.5 cm) was placed in 50 ml of O_2-saturated aqueous solution consisting of 20 mmol $La(NO_3)_3$, 16 mmol $Co(NO_3)_2$, and 4 mmol $Fe(NO_3)_3$ as the working electrode. The electrodeposition was carried out at 0.7 V versus saturated calomel electrode (SCE) for 300 s. The NF deposited with perovskite hydroxides was washed three times with deionized water and then ethanol, respectively, and dried in air at 80°C for 2 hours. Then, the as-prepared precursor was annealed at 700°C for 3 hours under flowing Ar (100 standard cubic centimeters per minute) with a heating rate of 5.0°C min^{-1}. The NF/oLCFO-Ar was obtained after calcination in Ar.

NF + oLCFO was fabricated by coating perovskite oxide oLCFO onto NF. The perovskite oxide oLCFO was prepared by sonicating perovskite hydroxides from the as-prepared NF/oLCFO-Ar precursor and annealing in air under other identical conditions. Then, the perovskite oxide oLCFO was dispersed in ethanol and impregnated onto NF with a loading mass similar to that of NF/oLCFO-Ar (1.10 mg cm^{-2}) to afford a reasonable comparison. The areal loading of the electrocatalyst was determined by comparing the mass of NF with or without perovskite oxide. NF/oLCFO-Air was synthesized through the same electrodeposition method but annealed in air under otherwise identical conditions. NF/rLCFO-Ar was electrodeposited in a N_2-saturated aqueous solution with the same composition and annealed under identical conditions as NF/oLCFO-Ar. A summary of preparation methods of electrocatalysts in this contribution is shown as table S2.

Characterization

The morphology and structure of the as-prepared samples were characterized using a JSM-7401F (3.0 kV; JEOL Ltd.) SEM and a JEM-2010 (120.0 kV; JEOL Ltd.) TEM. EDS analysis was performed at the acceleration voltage of 120.0 kV using a JEM-2010 TEM equipped with an Oxford Instruments EDS. XRD patterns were recorded on a Bruker D8 ADVANCE diffractometer at 40.0 kV and 120 mA with Cu-K_α radiation. XPS measurements were performed by ESCALAB 250Xi, with all XPS spectra corrected using the C 1s line at 284.6 eV.

Electrochemical evaluation

Electrochemical measurements were carried out on a three-electrode system controlled by a CHI-760D electrochemical workstation (CH Instruments) in O_2-saturated 0.10 M KOH electrolyte at room temperature. As for the three-electrode system, the as-prepared samples served directly as the working electrode clamped by a platinum electrode holder, with a platinum sheet electrode and an SCE as the counter electrode and reference electrode, respectively. All potentials measured were calibrated to RHE using the following equation: $E_{RHE} = E_{SCE} + 0.241\ V + 0.0592\ pH$. All current densities were normalized by geometrical electrode area.

OER performance of the electrocatalysts was evaluated using LSV with a potential range from 0.00 to 0.80 V versus SCE at a scan rate of 10.0 mV s^{-1}, and all the polarization profiles were corrected with 95% *iR*-compensation. The stability of the electrocatalysts was tested at a constant voltage required to reach an initial current density of 2.0 mA cm^{-2}.

SUPPLEMENTARY MATERIALS

Supplementary material for this article is available at http://advances.sciencemag.org/cgi/content/full/2/10/e1600495/DC1

fig. S1. XPS survey spectrum of NF/oLCFO-Ar.
fig. S2. EDS pattern of NF/oLCFO-Ar.
fig. S3. TEM imaging and corresponding EDS mapping of NF/oLCFO-Ar.
fig. S4. Morphology characterization of NF + oLCFO.
fig. S5. Stoichiometry characterization of perovskite oLCFO for NF + oLCFO and NF/oLCFO-Air.
fig. S6. OER performance of NF + oLCFO, NF/oLCFO-Air, and NF/rLCFO-Ar as control samples.
fig. S7. Morphology characterization of NF/oLCFO-Air.
fig. S8. Morphology characterization of NF/rLCFO-Ar.
fig. S9. XRD patterns of NF/rLCFO-Ar, NF/oLCFOH, and NF/rLCFOH perovskite hydroxide precursor.
fig. S10. Stoichiometry characterization of perovskite oxide nanoparticles of NF/rLCFO-Ar.
fig. S11. High-resolution (A) La 3d XPS spectrum and (B) Fe 2p XPS spectrum of NF/oLCFO-Ar, oLCFO perovskite oxide nanoparticles for NF + oLCFO and NF/oLCFO-Air, and NF/rLCFO-Ar.
table S1. Summary of OER performance for comparison of in situ–hybridized NF/oLCFO-Ar with transition metal oxides/hydroxides.
table S2. Summary of the preparation methods of hybrid electrocatalysts.

REFERENCES AND NOTES

1. J. A. Turner, Sustainable hydrogen production. *Science* **305**, 972–974 (2004).
2. H. B. Gray, Powering the planet with solar fuel. *Nat. Chem.* **1**, 7 (2009).
3. A. Kudo, Y. Miseki, Heterogeneous photocatalyst materials for water splitting. *Chem. Soc. Rev.* **38**, 253–278 (2009).
4. B. C. H. Steele, A. Heinzel, Materials for fuel-cell technologies. *Nature* **414**, 345–352 (2001).
5. K. Maeda, K. Teramura, D. L. Lu, T. Takata, N. Saito, Y. Inoue, K. Domen, Photocatalyst releasing hydrogen from water - Enhancing catalytic performance holds promise for hydrogen production by water splitting in sunlight. *Nature* **440**, 295 (2006).
6. M. G. Walter, E. L. Warren, J. R. McKone, S. W. Boettcher, Q. Mi, E. A. Santori, N. S. Lewis, Solar water splitting cells. *Chem. Rev.* **110**, 6446–6473 (2010).
7. F. Cheng, J. Chen, Metal–air batteries: From oxygen reduction electrochemistry to cathode catalysts. *Chem. Soc. Rev.* **41**, 2172–2192 (2012).
8. H. Ma, B. Wang, A bifunctional electrocatalyst α-MnO_2-$LaNiO_3$/carbon nanotube composite for rechargeable zinc–air batteries. *RSC Adv.* **4**, 46084–46092 (2014).
9. T. Y. Ma, J. Ran, S. Dai, M. Jaroniec, S. Z. Qiao, Phosphorus-doped graphitic carbon nitrides grown in situ on carbon-fiber paper: Flexible and reversible oxygen electrodes. *Angew. Chem. Int. Ed.* **54**, 4646–4650 (2015).
10. Y. Jiao, Y. Zheng, M. Jaroniec, S. Z. Qiao, Design of electrocatalysts for oxygen- and hydrogen-involving energy conversion reactions. *Chem. Soc. Rev.* **44**, 2060–2086 (2015).
11. D. Galizzio, F. Tantardi, S. Trasatti, Ruthenium dioxide: A new electrode material. I. Behaviour in acid solutions of inert electrolytes. *J. Appl. Electrochem.* **4**, 57–67 (1974).
12. Y. Lee, J. Suntivich, K. J. May, E. E. Perry, Y. Shao-Horn, Synthesis and activities of rutile IrO_2 and RuO_2 nanoparticles for oxygen evolution in acid and alkaline solutions. *J. Phys. Chem. Lett.* **3**, 399–404 (2012).
13. Z. Lu, W. Xu, W. Zhu, Q. Yang, X. Lei, J. Liu, Y. Li, X. Sun, X. Duan, Three-dimensional NiFe layered double hydroxide film for high-efficiency oxygen evolution reaction. *Chem. Commun.* **50**, 6479–6482 (2014).
14. M. Zhang, M. de Respinis, H. Frei, Time-resolved observations of water oxidation intermediates on a cobalt oxide nanoparticle catalyst. *Nat. Chem.* **6**, 362–367 (2014).
15. Z. Zhao, H. Wu, H. He, X. Xu, Y. Jin, A high-performance binary Ni–Co hydroxide-based water oxidation electrode with three-dimensional coaxial nanotube array structure. *Adv. Funct. Mater.* **24**, 4698–4705 (2014).
16. M. S. Burke, M. G. Kast, L. Trotochaud, A. M. Smith, S. W. Boettcher, Cobalt–iron (oxy) hydroxide oxygen evolution electrocatalysts: The role of structure and composition on activity, stability, and mechanism. *J. Am. Chem. Soc.* **137**, 3638–3648 (2015).
17. M. Gong, H. Dai, A mini review of NiFe-based materials as highly active oxygen evolution reaction electrocatalysts. *Nano Res.* **8**, 23–39 (2015).
18. H. Hu, B. Guan, B. Xia, X. W. Lou, Designed formation of Co_3O_4/$NiCo_2O_4$ double-shelled nanocages with enhanced pseudocapacitive and electrocatalytic properties. *J. Am. Chem. Soc.* **137**, 5590–5595 (2015).
19. R. N. Singh, S. K. Tiwari, S. P. Singh, N. K. Singh, G. Poillerat, P. Chartier, Synthesis of (La, Sr)CoO_3 perovskite films via a sol–gel route and their physicochemical and electrochemical surface characterization for anode application in alkaline water electrolysis. *J. Chem. Soc. Faraday Trans.* **92**, 2593–2597 (1996).
20. R. N. Singh, S. K. Tiwari, S. P. Singh, A. N. Jain, N. K. Singh, Electrocatalytic activity of high specific surface area perovskite-type $LaNiO_3$ via sol–gel route for electrolytic oxygen evolution in alkaline solution. *Int. J. Hydrogen Energy* **22**, 557–562 (1997).
21. A. R. Howells, A. Sankarraj, C. Shannon, A diruthenium-substituted polyoxometalate as an electrocatalyst for oxygen generation. *J. Am. Chem. Soc.* **126**, 12258–12259 (2004).
22. J. Suntivich, K. J. May, H. A. Gasteiger, J. B. Goodenough, Y. Shao-Horn, A perovskite oxide optimized for oxygen evolution catalysis from molecular orbital principles. *Science* **334**, 1383–1385 (2011).
23. K. J. May, C. E. Carlton, K. A. Stoerzinger, M. Risch, J. Suntivich, Y.-L. Lee, A. Grimaud, Y.-L. Shao-Horn, Influence of oxygen evolution during water oxidation on the surface of perovskite oxide catalysts. *J. Phys. Chem. Lett.* **3**, 3264–3270 (2012).
24. B. Han, M. Risch, Y.-L. Lee, C. Ling, H. Jia, Y. Shao-Horn, Activity and stability trends of perovskite oxides for oxygen evolution catalysis at neutral pH. *Phys. Chem. Chem. Phys.* **17**, 22576–22580 (2015).
25. R. Liu, F. Liang, W. Zhou, Y. Yang, Z. Zhu, Calcium-doped lanthanum nickelate layered perovskite and nickel oxide nano-hybrid for highly efficient water oxidation. *Nano Energy* **12**, 115–122 (2015).
26. W. Zhou, M. Zhao, F. Liang, S. C. Smith, Z. Zhu, High activity and durability of novel perovskite electrocatalysts for water oxidation. *Mater. Horiz.* **2**, 495–501 (2015).
27. J.-I. Jung, H. Y. Jeong, M. G. Kim, G. Nam, J. Park, J. Cho, Fabrication of $Ba_{0.5}Sr_{0.5}Co_{0.8}Fe_{0.2}O_{3-\delta}$ catalysts with enhanced electrochemical performance by removing an inherent heterogeneous surface film layer. *Adv. Mater.* **27**, 266–271 (2015).
28. C. Su, W. Wang, Y. Chen, G. Yang, X. Xu, M. O. Tadé, Z. Shao, $SrCo_{0.9}Ti_{0.1}O_{3-\delta}$ as a new electrocatalyst for the oxygen evolution reaction in alkaline electrolyte with stable performance. *ACS Appl. Mater. Interfaces* **7**, 17663–17670 (2015).
29. H. W. Park, D. U. Lee, P. Zamani, M. H. Seo, L. F. Nazar, Z. Chen, Electrospun porous nanorod perovskite oxide/nitrogen-doped graphene composite as a bi-functional catalyst for metal air batteries. *Nano Energy* **10**, 192–200 (2014).
30. X. Ge, F. W. T. Goh, B. Li, T. S. A. Hor, J. Zhang, P. Xiao, X. Wang, Y. Zong, Z. Liu, Efficient and durable oxygen reduction and evolution of a hydrothermally synthesized $La(Co_{0.55}Mn_{0.45})O_{3-\delta}$ nanorod/graphene hybrid in alkaline media. *Nanoscale* **7**, 9046–9054 (2015).
31. H. Zhao, C. Chen, D. Chen, M. Saccoccio, J. Wang, Y. Gao, T. H. Wan, F. Ciucci, $Ba_{0.95}La_{0.05}FeO_{3-\delta}$–multi-layer graphene as a low-cost and synergistic catalyst for oxygen evolution reaction. *Carbon* **90**, 122–129 (2015).
32. D. U. Lee, M. G. Park, H. W. Park, M. H. Seo, V. Ismayilov, R. Ahmed, Z. Chen, Highly active Co-doped $LaMnO_3$ perovskite oxide and N-doped carbon nanotube hybrid bi-functional catalyst for rechargeable zinc–air batteries. *Electrochem. Commun.* **60**, 38–41 (2015).
33. K. Elumeeva, J. Masa, F. Tietz, F. Yang, W. Xia, M. Muhler, W. Schuhmann, A simple approach towards high-performance perovskite-based bifunctional oxygen electrocatalysts. *ChemElectroChem* **3**, 138–143 (2016).
34. C. Tang, H.-S. Wang, H.-F. Wang, Q. Zhang, G.-L. Tian, J.-Q. Nie, F. Wei, Spatially confined hybridization of nanometer-sized NiFe hydroxides into nitrogen-doped graphene frameworks leading to superior oxygen evolution reactivity. *Adv. Mater.* **27**, 4516–4522 (2015).
35. X. Zhu, C. Tang, H.-F. Wang, Q. Zhang, C. Yang, F. Wei, Dual-sized NiFe layered double hydroxides in situ grown on oxygen-decorated self-dispersal nanocarbon as enhanced water oxidation catalysts. *J. Mater. Chem. A* **3**, 24540–24546 (2015).
36. H.-F. Wang, C. Tang, Q. Zhang, Towards superior oxygen evolution through graphene barriers between metal substrates and hydroxide catalysts. *J. Mater. Chem. A* **3**, 16183–16189 (2015).
37. Z. Li, M. Shao, H. An, Z. Wang, S. Xu, M. Wei, D. G. Evans, X. Duan, Fast electrosynthesis of Fe-containing layered double hydroxide arrays toward highly efficient electrocatalytic oxidation reactions. *Chem. Sci.* **6**, 6624–6631 (2015).
38. X. Lu, C. Zhao, Electrodeposition of hierarchically structured three-dimensional nickel–iron electrodes for efficient oxygen evolution at high current densities. *Nat. Commun.* **6**, 6616 (2015).
39. X. Yu, M. Zhang, W. Yuan, G. Shi, A high-performance three-dimensional Ni–Fe layered double hydroxide/graphene electrode for water oxidation. *J. Mater. Chem. A* **3**, 6921–6928 (2015).
40. A. Feldhoff, M. Arnold, J. Martynczuk, T. M. Gesing, H. Wang, The sol–gel synthesis of perovskites by an EDTA/citrate complexing method involves nanoscale solid state reactions. *Solid State Sci.* **10**, 689–701 (2008).
41. J. Zhu, A. Thomas, Perovskite-type mixed oxides as catalytic material for NO removal. *Appl. Catal. B Environ.* **92**, 225–233 (2009).
42. M. Liu, R. Wang, D. F. Li, D. T. Liang, A novel combustion route for the preparation of perovskite-type oxygen permeable materials. *Mater. Chem. Phys.* **102**, 132–139 (2007).
43. Y. Zhu, W. Zhou, Z.-G. Chen, Y. Chen, C. Su, M. O. Tadé, Z. Shao, $SrNb_{0.1}Co_{0.7}Fe_{0.2}O_{3-\delta}$ perovskite as a next-generation electrocatalyst for oxygen evolution in alkaline solution. *Angew. Chem. Int. Ed. Engl.* **54**, 3897–3901 (2015).
44. F. Song, K. Schenk, X. Hu, A nanoporous oxygen evolution catalyst synthesized by selective electrochemical etching of perovskite hydroxide $CoSn(OH)_6$ nanocubes. *Energy Environ. Sci.* **9**, 473–477 (2016).
45. A. J. Esswein, M. J. McMurdo, P. N. Ross, A. T. Bell, T. D. Tilley, Size-dependent activity of Co_3O_4 nanoparticle anodes for alkaline water electrolysis. *J. Phys. Chem. C* **113**, 15068–15072 (2009).

46. H. W. Park, D. U. Lee, M. G. Park, R. Ahmed, M. H. Seo, L. F. Nazar, Z. W. Chen, Perovskite–nitrogen-doped carbon nanotube composite as bifunctional catalysts for rechargeable lithium–air batteries. *ChemSusChem* **8**, 1058–1065 (2015).
47. M. W. Kanan, J. Yano, Y. Surendranath, M. Dincă, V. K. Yachandra, D. G. Nocera, Structure and valency of a cobalt–phosphate water oxidation catalyst determined by in situ x-ray spectroscopy. *J. Am. Chem. Soc.* **132**, 13692–13701 (2010).
48. L. Trotochaud, J. K. Ranney, K. N. Williams, S. W. Boettcher, Solution-cast metal oxide thin film electrocatalysts for oxygen evolution. *J. Am. Chem. Soc.* **134**, 17253–17261 (2012).
49. M. Risch, A. Grimaud, K. J. May, K. A. Stoerzinger, T. J. Chen, A. N. Mansour, Y. Shao-Horn, Structural changes of cobalt-based perovskites upon water oxidation investigated by EXAFS. *J. Phys. Chem. C* **117**, 8628–8635 (2013).
50. D.-D. Zhao, S.-J. Bao, W.-J. Zhou, H.-L. Li, Preparation of hexagonal nanoporous nickel hydroxide film and its application for electrochemical capacitor. *Electrochem. Commun.* **9**, 869–874 (2007).
51. C. Yuan, J. Li, L. Hou, X. Zhang, L. Shen, X. W. Lou, Ultrathin mesoporous $NiCo_2O_4$ nanosheets supported on Ni foam as advanced electrodes for supercapacitors. *Adv. Funct. Mater.* **22**, 4592–4597 (2012).
52. L. Fu, Z. Liu, Y. Liu, B. Han, P. Hu, L. Cao, D. Zhu, Beaded cobalt oxide nanoparticles along carbon nanotubes: Towards more highly integrated electronic devices. *Adv. Mater.* **17**, 217–221 (2005).

Acknowledgments

Funding: Q.Z. acknowledges support from the Ministry of Science and Technology of the People's Republic of China (grant no. 2016YFA0202500), the National Natural Science Foundation of China (grant nos. 21306102 and 21422604), and the Tsinghua University Initiative Scientific Research Program (grant no. 20161080166). **Author contributions:** Q.Z. conceived the idea. B.-Q.L. and C.T. carried out the materials synthesis and electrochemical testing. B.-Q.L., H.-F.W., and X.-L.Z. characterized the materials. B.-Q.L., C.T., and Q.Z. cowrote the manuscript. All authors contributed to and commented on this article. Q.Z. proposed the research direction and supervised the project. **Competing interests:** The authors declare that they have no competing interests. **Data and materials availability:** All data needed to evaluate the conclusions in the paper are present in the paper and/or the Supplementary Materials. Additional data related to this paper may be requested from the authors.

Submitted 8 March 2016
Accepted 22 September 2016
Published 21 October 2016
10.1126/sciadv.1600495

Citation: B.-Q. Li, C. Tang, H.-F. Wang, X.-L. Zhu, Q. Zhang, An aqueous preoxidation method for monolithic perovskite electrocatalysts with enhanced water oxidation performance. *Sci. Adv.* **2**, e1600495 (2016).

An aqueous preoxidation method for monolithic perovskite electrocatalysts with enhanced water oxidation performance

Bo-Quan Li, Cheng Tang, Hao-Fan Wang, Xiao-Lin Zhu and Qiang Zhang

Sci Adv **2** (10), e1600495.
DOI: 10.1126/sciadv.1600495